Soft Matter

PAPER

View Article Online
View Journal | View Issue

Cite this: *Soft Matter*, 2020, **16**, 5431

Diffusion properties of self-propelled particles in cellular flows

Lorenzo Caprini, *[ab] Fabio Cecconi,[c] Andrea Puglisi[d] and Alessandro Sarracino[e]

Received 15th March 2020,
Accepted 20th May 2020

DOI: 10.1039/d0sm00450b

rsc.li/soft-matter-journal

We study the dynamics of a self-propelled particle advected by a steady laminar flow. The persistent motion of the self-propelled particle is described by an active Ornstein–Uhlenbeck process. We focus on the diffusivity properties of the particle as a function of persistence time and free-diffusion coefficient, revealing non-monotonic behaviors, with the occurrence of a minimum and a steep growth in the regime of large persistence time. In the latter limit, we obtain an analytical prediction for the scaling of the diffusion coefficient with the parameters of the active force. Our study sheds light on the effect of a flow-field on the diffusion of active particles, such as living microorganisms and motile phytoplankton in fluids.

1 Introduction

In recent years, great interest has been raised by the complex dynamics of biological microorganisms or artificial microswimmers, which convert energy from the environment into systematic motion.[1,2] Nowadays, these non-equilibrium systems are classified as self-propelled particles (SPP), a subclass of dry active matter. The behavior of SPP without environmental constraints has been largely studied and has shown a very fascinating phenomenology, such as: swarming, clustering,[3–5] phase-separation,[6–11] spontaneous velocity alignments[12–14] and vortex formation.[15] These phenomena have not a passive Brownian counterpart, because of the intrinsic non-equilibrium nature of the self-propelled motion, characterized by a persistence time τ, and, in particular, due to the peculiar interplay between active forces and interactions among particles. Even in non-interacting cases, the diffusive properties of SPP have been a matter of intense study both experimentally and numerically since the self-propulsion enhances the diffusivity with respect to any passive tracers.[16–21]

The dynamics of SPP in complex environments constitutes a central issue for its great biological interest. Indeed, in Nature, microswimmers or bacteria, when encounter soft or solid obstacles[22] or even hard walls,[23] accumulate in front of them producing interesting patterns.[24–28] Moreover, the swimming in porous soil,[29] blood flow[30] or biological tissues[31] constitutes other contexts of investigation. Thus, the description of the active dynamics beyond homogeneous environments represents a great challenge towards the comprehension of the life of microorganisms in their habitat. Moreover, the recent technological advances have led to the possibility of manufacturing complex patterns of irregular or regular structures of micro-obstacles that mimic the cellular environment or, more generally, the medium where SPP move.[32–36] The dynamics in complex environments has been studied for instance in mazes,[37] pinning substrates,[38] arrays of funnels,[39–43] comb lattices,[44] fixed arrays of pillars[45–48] or even in systems with random moving obstacles,[49,50] leading in some cases to anomalous diffusion.[51–53]

Another important issue concerns the dynamics and diffusion properties of SPP in the presence of a non-uniform velocity field. In the case of passive Brownian particles, the problem has been largely studied, both for laminar and turbulent flows.[54] The simplest example of the interplay between advection and molecular diffusion is the Taylor dispersion[55] which is observed in a channel with a Poiseuille flow. In the case of SPP, similar studies have great relevance in describing the behavior of microscopic living organisms such as certain kinds of motile plankton and microalgae. For instance, the distribution of SPP in convective fluxes is a problem that comes from the observations that plankton is subject to Langmuir circulation.[56,57] For gyrotactic swimmers, such as certain motile phytoplanktons and microalgae, the motion in the presence of flow fields, both in laminar and turbulent regimes, has been studied in ref. 58 and 59, showing that strong heterogeneity in the distribution of particles can occur. Interaction between laminar flow and motility has been studied also in bacteria, with the observation of interesting trapping phenomena[60] and complex particle trajectories.[61]

[a] *Gran Sasso Science Institute (GSSI), Via. F. Crispi 7, 67100 L'Aquila, Italy. E-mail: lorenzo.caprini@gssi.it*
[b] *Scuola di Scienze e Tecnologie, Università di Camerino – via Madonna delle Carceri, 62032 Camerino, Italy*
[c] *Istituto dei Sistemi Complessi-CNR, Via Taurini 19, I-00185, Rome, Italy*
[d] *Istituto dei Sistemi Complessi-CNR, P.le A. Moro, I-00185, Rome, Italy*
[e] *Dipartimento di Ingegneria, Università della Campania "L. Vanvitelli", via Roma 29, 81031 Aversa (Caserta), Italy*

From the theoretical point of view, in the passive Brownian case, the effective diffusion coefficient, D_{eff}, of a tracer advected by a laminar flow has been computed analytically in the limit of small diffusivity by Shraiman.[54] In this case, D_{eff} is larger than the free-diffusion coefficient D_0 (the diffusivity in the absence of convective flow). A first-order correction accounting for the noise persistence has been computed by Castiglione and Crisanti,[62] who estimated asymptotically D_{eff} for vanishing persistence time, finding a further enhancement of diffusivity.

In this manuscript, we generalize the study of the diffusion of SPP in the presence of laminar flows, for large values of the persistence time τ. The effect of an underlying cellular flow has been considered for instance in ref. 63, revealing non-trivial effects such as negative differential and absolute mobility when the particles are subject to external forces.[64–69] At variance with,[63] where concentration in some flow regions was investigated, we focus here on the transport properties, such as the diffusion coefficient and the mean square displacement. Our analysis unveils a rich phenomenology, characterized by a nonmonotonic behavior of D_{eff} as a function of the persistence time of the active force. This implies that, in some cases, the coupling of the active force with the underlying velocity field can trap the SPP, resulting in a decrease of diffusivity. The dynamics of active particles in convective rolls has recently been considered in ref. 70 where the authors focus on the role of chirality.

The paper is structured as follows: after the introduction of the model in Section 2, we present our numerical results in Section 3, focusing on the mean square displacement and effective diffusion coefficient as a function of the model parameters. In Section 4, we present an analytical computation which explains the behavior of D_{eff} in the large persistence regime. Then, we summarize the result in the conclusive section.

2 The model

We consider a dilute system of active particles in two dimensions diffusing in a cellular flow. The position, $\mathbf{r} = (x,y)$, of the tagged SPP is described by the following stochastic differential equation:

$$\dot{\mathbf{r}} = \mathbf{A}(\mathbf{r}) + \mathbf{w}, \tag{1}$$

where we have neglected the thermal Brownian motion due to the solvent and also any inertial effects, as usual in these systems.[1] The self-propulsion mechanism is represented by the term $\mathbf{w}$, evolving according to the Active Ornstein–Uhlenbeck particle (AOUP) dynamics. AOUP is an established model to describe the behavior of SPP[71–77] or passive particles immersed into an active bath.[78,79] The colored noise, $\mathbf{w}$, models the persistent motion of a SPP conferring time-persistence to a single trajectory and evolves according to the equation

$$\tau\dot{\mathbf{w}} = -\mathbf{w} + \sqrt{2D_0}\xi, \tag{2}$$

where τ is the auto-correlation time of $\mathbf{w}$ and sets the persistence of the dynamics, while the constant D_0 represents the effective diffusion due to the self-propulsion in a homogeneous environment. The ratio $\sqrt{D_0/\tau}$ determines the average velocity induced by the self-propulsion, being D_0/τ the variance of $\mathbf{w}$.

The cellular flow, $\mathbf{A}$, is chosen as a periodic, divergenceless field obtained from the stream function

$$\psi(\mathbf{r}) = \frac{U_0}{k}\sin(kx)\sin(ky), \tag{3}$$

where U_0 sets the maximal intensity of the field, while $k = 2\pi/L$ determines the cell periodicity, with L the cell size. The flow is obtained from the stream function as

$$(A_x,A_y) = \{\partial_y\psi(\mathbf{r}), -\partial_x\psi(\mathbf{r})\}. \tag{4}$$

In practice, the flow is a square lattice of convective cells (vortices) with alternated directions of rotation. The boundary lines separating neighboring cells are called ''separatrices'': along a separatrix, the flow has a maximal velocity in the parallel direction and zero in the perpendicular one. The structure of the cellular flow introduces a time-scale in the dynamics of the system, the turnover time $T_{\mathrm{U}} = L/U_0$, *i.e.* the time needed by a particle, in the absence of any other forces, to explore the whole periodicity of the system. The self-propulsion is characterized by the typical time τ, whose interplay with T_{U} determines a complex phenomenology, both at the level of a single particle trajectory and at the diffusive level, as it will be illustrated in the next sections.

We remark that a self-propelled particle immersed in flow cannot be studied employing any suitable approximations, such as the unified colored noise approximation,[80,81] except for the small persistence regime, defined for values of τ such that $\tau < \tau^* = 1/kU_0 = T_{\mathrm{U}}/2\pi$, as shown in Appendix A. Indeed, the form of the velocity dynamics in the large persistence regime prevents the possibility of adapting the adiabatic elimination, except in the limit of small τ.[82]

3 Numerical results

We carry out a numerical study of the active dynamics (1) and (2) that are integrated *via* a second order stochastic Runge–Kutta algorithm[83] with a time step $h = 10^{-3}$ and for a time at least $2 \times 10^2\tau$. Simulations are performed keeping fixed the cellular structure, $L = 1$, $U_0 = 1$, in such a way that $T_{\mathrm{U}} = 1$, *i.e.* measuring positions and times in unit of L and T_{U}. We evaluate the influence of the parameters τ and D_0 on the dynamics. The generality of this procedure is shown in Appendix B: introducing dimensionless variables, a change of L or U_0 can be recast onto a variation of the self-propulsion parameters.

3.1 Single particle trajectories

We start by studying qualitatively the typical trajectories of the SPP in different relevant regimes. These observations will help us to understand the average properties showed by the mean square displacement and by the diffusion coefficient. In particular, in Fig. 1(a), we compare different single-particle trajectories obtained for three different values of $\tau = 10^{-1}$, 1, 10 at fixed $D_0 = 10^{-2}$. For $\tau \ll T_{\mathrm{U}}$ (yellow trajectory), the persistence feature of the self-propulsion is not relevant since $\mathbf{w}$ changes direction many times inside a single cell. As a consequence, the self-propulsion is

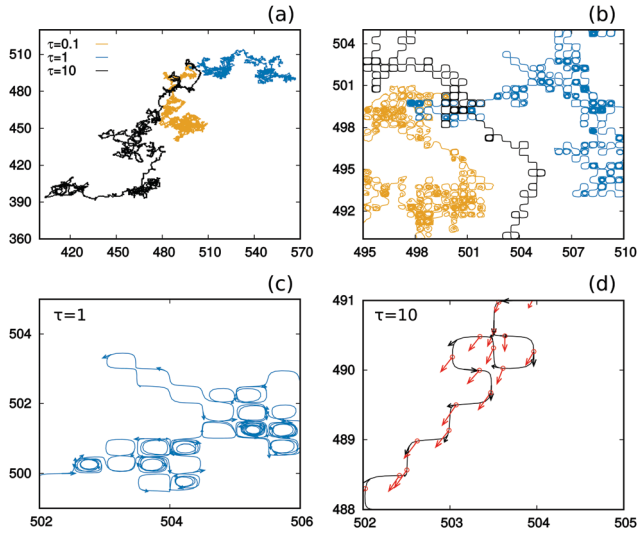

Fig. 1 (a and b) panels: Snapshot of the trajectories for different values of τ = 0.1, 1, 10. (c and d) panels: Enlargement for τ = 1 (c) and for τ = 10 (d). In panel (c) the arrows represent the velocity of the particle. In panel (c), the black arrows denote the velocity, while the red arrows denote the self-propulsion. The self-propulsion is rescaled for presentation reasons but here is $\sim 10^{-2}$ smaller than U_0. Simulations are realized with $D_0 = 10^{-2}$. The other parameters are U_0 = 1 and L = 1.

indistinguishable from a thermal noise with diffusivity D_0 (see Section (3.3)).

For $\tau \gg T_U$ (black trajectory), the self-propulsion changes only after that the particle has crossed many cells. In these regimes, the average speed of self-propulsion is very small and decreases as $1/\sqrt{\tau}$ since D_0 is fixed. As shown in panels (b) and (d) of Fig. 1, the particle proceeds along the separatrix between different vortices, and explores the regions where the cellular flow assumes its maximal value. The particle does not explore the region inside the cell and quite rarely becomes trapped in a vortex. This event becomes rarer as τ increases. As a consequence, the self-propelled particle moves in a zig-zag-like way with a trajectory displaying an almost deterministic behavior that follows the flow field as shown in Fig. 1(d). Due to the small value of the self-propulsion compared to U_0, $\mathbf{w}$ plays a role only in a small region near the nodes of the separatrix (where the flow field is zero). In those regions, the direction of $\mathbf{w}$ determines which one of the two separatrices the particle will follow. Moreover, since the average change of the self-propulsion direction is ruled by τ, the same separatrix will be preferred for times smaller than τ. This results in a unidirectional motion (along the separatrices) for small times ($<\tau$), in analogy with a free active particle with velocity U_0, while a diffusive-like behavior will be obtained for times larger than T_U.

For intermediate values of τ, *i.e.* when $\tau \sim T_U$, the trajectory is more complicated, as illustrated in Fig. 1(c). The self-propulsion can deviate the trajectory from the streamlines, pushing the SPP inside a vortex. The exit from the vortex can be determined by a fluctuation of the self-propulsion. A particle needs more time with respect to the thermal case to escape and proceed along the separatrix.

3.2 Mean square displacement

The rescaled mean square displacement (MSD) of the SPP, $\langle[\mathbf{r}(t) - \mathbf{r}(0)]^2\rangle/2t$, averaged over thousands of realizations, is reported for several values of τ and three values of D_0 (Fig. 2(a)–(c)). The MSD(t) reflects the behaviors of the single-particle trajectories: we identify a short-time ballistic growth, an intermediate-time nonmonotonic crossover and a final long-time diffusive regime. In the small-τ limit, such that $\tau < \tau^*$, ballistic regimes occur for $t < \tau$ (not shown in the figure), in analogy with active particles in a homogeneous environment.[21] When $\tau > \tau^*$, deviations from ballistic regimes occur for $t > \tau^*$, as reported in Fig. 2(a)–(c). As shown in each panel, this regime weakly depends on τ and D_0 since for small t the MSD collapses onto the same curve, at variance with active particles in homogeneous environments. A second regime occurs in the range of times $\tau^* < t < \tau$, until a maximum of $\langle[\mathbf{r}(t) - \mathbf{r}(0)]^2\rangle/2t$ is observed for $t \sim \tau$. After this maximum, the diffusivity slows down and approaches normal diffusion asymptotically. The comparison between the different panels of Fig. 2 suggests that the intermediate crossover regimes

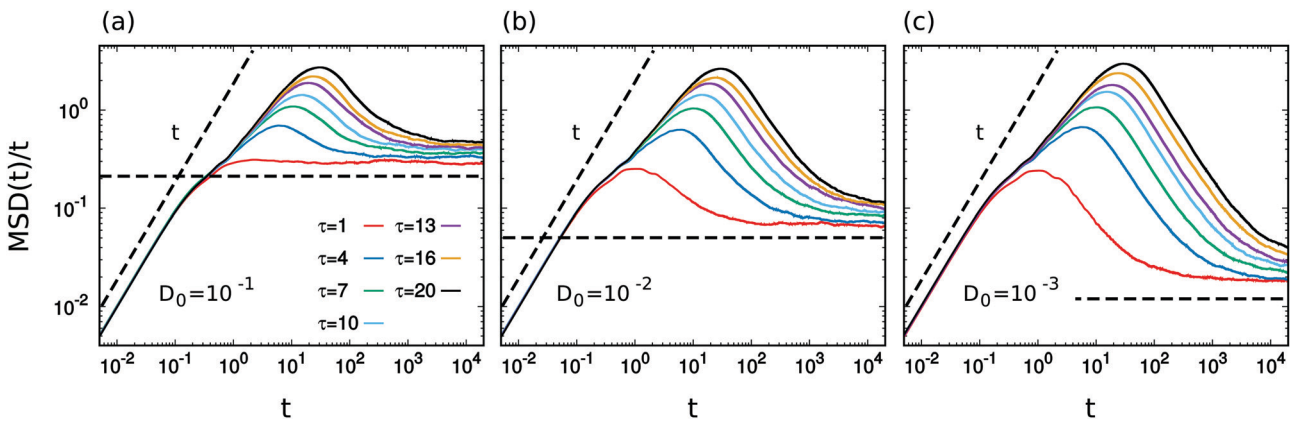

Fig. 2 MSD(t)/t as a function of t for different values of τ, namely τ = 1, 4, 7, 10, 13, 16, 20 from the bottom to the top as shown in the legend. Panels (a–c) are obtained with three different values of $D_0 = 10^{-1}$, 10^{-2}, 10^{-3} from the left to the right. Dashed black lines mark linear and constant behaviors (corresponding on the ballistic and diffusive regimes of the MSD(t), respectively). The other parameters are U_0 = 1 and L = 1.

are less pronounced as D_0 increases even if, in all the cases, the nonmonotonic crossover region enlarges as τ grows. At large times, after $t > \tau_D$, the diffusive behavior is reached. Remarkably, the transient regime has a quite long duration, and the typical time τ_D increases with τ and decreases with D_0. We remark that the slowing down of the dynamics at intermediate times is related to the trapping effect due to the vortices of the cellular flow, which confines the particle motion in a limited region for a certain time.

3.3 Diffusion coefficient

To unveil the effect of the self-propulsion force on the long-time diffusive dynamics, we study the diffusion coefficient

$$D_{\text{eff}} = \lim_{t\to\infty} \frac{1}{4t}\left\langle [\mathbf{r}(t) - \mathbf{r}(0)]^2 \right\rangle, \tag{5}$$

as a function of the activity parameters, τ and D_0. The case $\tau = 0$ corresponds to the passive Brownian limit, where the leading contribution to the diffusion comes from the particles moving along the separatrices, and for which an analytical prediction has been computed by Shraiman in:[54]

$$D_{\text{eff}}(\tau = 0) = \frac{S(k=1)}{\sqrt{\pi}}\sqrt{\frac{U_0 L D_0}{2\pi}}. \tag{6}$$

Here, the factor $S(k)$ depends on the cell geometry and is reported in ref. 54. For the square-cell setup employed in the numerical study of this manuscript, we have $S(k=1)/\sqrt{\pi} \simeq 1.07$. We remark that the cellular flow enhances the diffusivity at small D_0, with respect to the case of homogeneous environments, producing a scaling $\sim \sqrt{D_0}$ instead of $\sim D_0$.

In Fig. 3, we plot $D_{\text{eff}}(\tau)/D_{\text{eff}}(0)$ as a function of τ for four values of D_0 to show the role of the self-propulsion persistence. As expected, at small values of τ, the prediction (6) is in agreement with numerical simulations since the self-propulsion acts as an effective thermal noise in this regime. Depending on the value of D_0, we observe a different phenomenology. In particular, at larger values of D_0, for instance $D_0 \geq 10^{-1}$, D_{eff} grows with τ and, thus, the increase of the persistence time enhances the diffusivity, even if the effective velocity decreases as $\sqrt{D_0/\tau}$. More surprisingly, for smaller values of D_0, we obtain a non-monotonic behavior: in a regime of τ comparable with T_U, starting from $\tau^* = 1/kU_0$, we observe that D_{eff} decreases down to a minimum value which is reached at times close to T_U. We remark that τ^* is the value of τ for which the overdamped approach for small τ does not hold, as shown in detail in Appendix A. After the minimum is reached, D_{eff} grows indefinitely. In particular, for τ large enough we observe $D_{\text{eff}} > D_{\text{eff}}(\tau = 0)$ as in the cases with larger D_0.

These observations are in agreement with the phenomenology characterizing the single-particle trajectories (Fig. 1). Indeed, the possibility for a particle to be trapped into a vortex for long times - seen for values of $\tau \sim T_U$ – is coherent with the observed reduction of D_{eff} in a range of τ. Also, the existence of trajectories running fast along the separatrices for large values of τ is consistent with the final growth of D_{eff} (asymptotically for large τ). Using this information, in the next section, we will derive an analytical prediction for D_{eff}, in the regime $\tau \gg T_U$.

In panel (a) of Fig. 4, we show D_{eff} as a function of D_0 for several values of τ to test Shraiman's scaling with D_0. As shown in panel (b) of Fig. 4, for $\tau \ll T_U$, $D_{\text{eff}} \sim \sqrt{D_0}$, in agreement with eqn (6). Shraiman's scaling breaks down for large values of D_0, where $D_{\text{eff}} \propto D_0$, occurring when $\mathbf{w}$ becomes comparable with

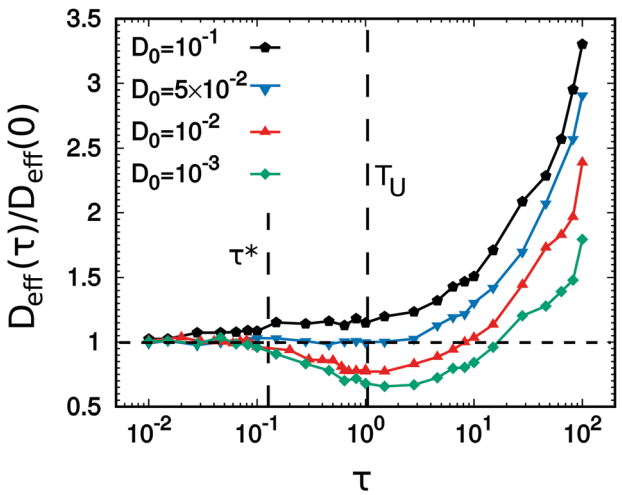

Fig. 3 Effective diffusion coefficient as a function of τ, for several values of D_0 as shown in the legend. The constant $D_{\text{eff}}(0)$ is calculated from eqn (6). The two dashed black lines are eye-guides to mark the value of τ^* and T_U. The other parameters are $U_0 = 1$ and $L = 1$.

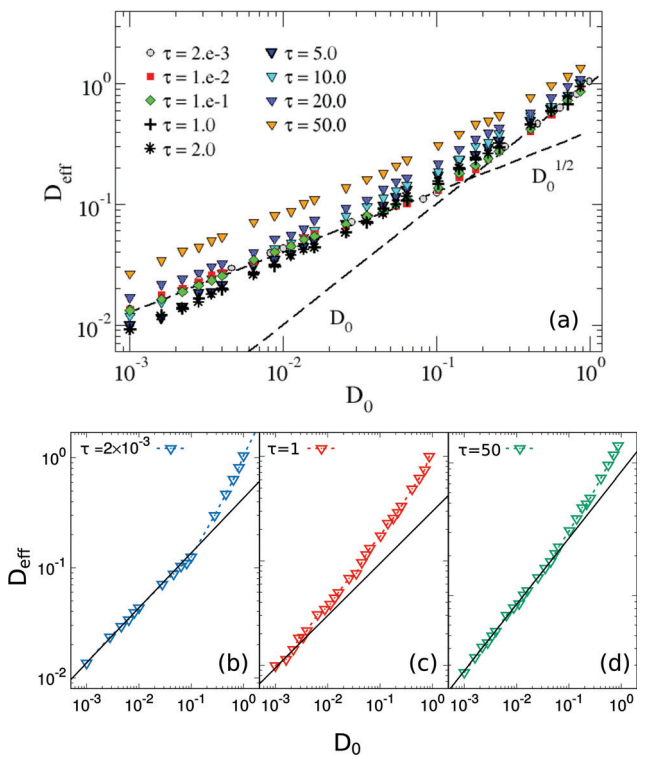

Fig. 4 Effective diffusion coefficient, D_{eff}, *vs.* D_0 for different values of τ, as shown in the legend (panel (a)). The dashed black lines are eye guides showing the behavior $\sim D_0$ and $\sim \sqrt{D_0}$. Panels (b–d) compare a curve of D_{eff} (for a given τ) with the behavior $\propto \sqrt{D_0}$. The other parameters are $U_0 = 1$ and $L = 1$.

U_0 and the cellular-flow plays a marginal role in the transport process. In Fig. 4(c), we observe that Shraiman's scaling does not hold for the intermediate values of τ (the region of τ corresponding to the minimum in Fig. 3), while it is recovered in the regime of large τ, namely for $\tau \gg T_U$, even if the values of $D_{\rm eff}$ are quite larger with respect to eqn (6), see panel (d).

4 Analytical prediction of $D_{\rm eff}$ for large persistence

In the large persistence regime, $\tau \gg T_U$, the study of the single-particle trajectory has revealed that the SPP runs almost deterministically along the separatrices choosing the "same" direction for a time of order τ. The change of direction occurs after a time $\sim\tau$, like for active particles in homogeneous environment. In this simple case, the MSD, at large times, is given by

$$\mathrm{MSD}(t \gg \tau) \approx \mathscr{L}^2 n = \left(\sqrt{D_0\tau}\right)^2 \frac{t}{\tau}, \tag{7}$$

where $\mathscr{L} = \sqrt{D_0\tau}$ is the persistence length and $n = t/\tau$ counts the number of persistence lengths covered by the free-particle in the time t.

To estimate the MSD of a SPP in the cellular flow, we replace $\mathscr{L}$ in eqn (7) with the effective persistence length, $\mathscr{L}_{\rm eff}$, of a particle moving along the separatrices, with velocity $U_0 \sin(kx)$ for $x \in [0,L/2]$ (obtained from eqn (1)). Thus, at large times, we get the estimate

$$\mathrm{MSD}(t \gg \tau) \approx \mathscr{L}_{\rm eff}{}^2 \frac{t}{\tau} = \left(\frac{L}{2\sqrt{2}} \frac{\tau}{t_s}\right)^2 \frac{t}{\tau}, \tag{8}$$

where t_s is the typical time to run for a distance $L/2$ along a separatrix and is calculated in Appendix C. We remark that the validity of eqn (8) is restricted to the regime $\tau \gg T_U$, where $\mathbf{w}$ plays a role only on the nodes of the separatrices because $|\mathbf{w}| < U_0$.

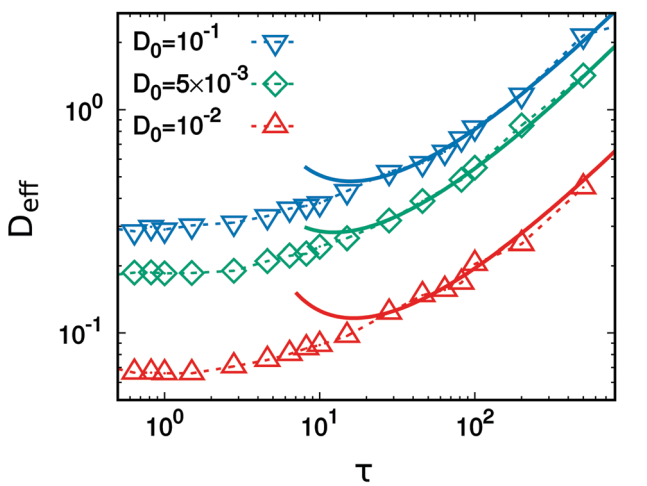

Fig. 5 Effective diffusion coefficient *vs.* τ for three different values of D_0 (colored data). The solid lines are obtained from numerical fits of the prediction (10), namely $g(\tau) = a\tau/\log^2(2U_0{}^2\tau/D_0/b)$, where a and b are two parameters. In particular, $b \simeq 6$ is a constant factor and does not depend on D_0 and T_U. The parameters of the numerical study are $U_0 = 1$ and $L = 1$.

This argument suggests that the diffusion coefficient increases linearly with τ and does not depend on D_0, except for a dependence contained in t_s. In particular, we get (see Appendix C)

$$t_s \approx \frac{L}{U_0 2\pi} \log\left[\frac{2}{b}\frac{\tau}{D_0}U_0{}^2\right], \tag{9}$$

in the limit $\sqrt{D_0}/\sqrt{\tau} \ll U_0$. The parameter b is a numerical factor independent of τ, D_0 and T_U. In this regime, the prediction for the diffusion coefficient, for $\tau \gg t_s$ (calculated for $t \gg \tau$), reads:

$$D_{\rm eff} \propto \frac{U_0{}^2\tau}{\log^2\left[\frac{2}{b}U_0{}^2\frac{\tau}{D_0}\right]}. \tag{10}$$

The comparison between prediction and numerical data is reported in Fig. 5 as a function of τ for three different values of D_0. The results are in good agreement for $\tau \gg T_U$, while marked deviations emerge for $\tau \sim T_U$, where the main hypothesis behind eqn (10) does not apply.

5 Conclusion

In this manuscript, we have studied the diffusive properties of a self-propelled particle moving in a steady laminar flow, assessing the effect of the self-propulsion. The diffusion coefficient displays a non-monotonic behavior as a function of the persistence time τ. In particular, a minimum occurs for a large range of D_0 when τ is comparable with the turnover time, followed by a sharp increase, faster than τ, such that the value of the diffusion coefficient exceeds Shraiman's prediction valid in the passive Brownian case. Such a mechanism is discussed and connected with the single-particle trajectory, specifically to the occurrence of a trapping mechanism into the vortices. Additionally, Shraiman's scaling with the diffusion coefficient is tested in the active case, revealing an intriguing scenario.

We expect our results are still valid (at least qualitatively) for another popular model which describes the behavior of self-propelled particles, *i.e.* the active Brownian particles model.[6,16] Its connection with the AOUP model, employed in this work, has been shown in ref. 71 and 84 and results from the shape of the time-autocorrelation of the self-propulsion which decays exponentially in both cases. Additionally, we remark that the observed phenomenology is mainly caused by the short-time persistence of the trajectory, a feature shared by both models.

Our study shows that the presence of the self-propulsion affects the diffusion in a steady laminar flow and could represent a mechanism naturally developed by self-propelled agents to improve the efficiency of the transport mechanism. Testing the presence of similar nonmonotonic behaviors in other laminar flow fields, going beyond the specific functional form adopted in this manuscript, could be a promising research line to understand the behavior of self-propelled microorganisms in their complex habitats.

Conflicts of interest

There are no conflicts to declare.

Appendix

A Failure of the UCNA approximation

By taking the time derivative of the equation of motion (1), we get:

$$\ddot{\mathbf{r}} = \nabla\mathbf{A}(\mathbf{r})\dot{\mathbf{r}} + \dot{\mathbf{w}} \tag{11}$$

$$\tau\dot{\mathbf{w}} = -\mathbf{w} + \sqrt{2D_0}\xi, \tag{12}$$

where the matrix $\nabla\mathbf{A}$ reads:

$$\nabla\mathbf{A} = kU_0\begin{bmatrix}\cos(kx)\cos(ky) & -\sin(kx)\sin(ky)\\ \sin(kx)\sin(ky) & -\cos(kx)\cos(ky)\end{bmatrix} = k^2\begin{bmatrix}\phi & -\psi\\ \psi & -\phi\end{bmatrix},$$

being ψ the stream function defined by eqn (3) and

$$\phi(\mathbf{r}) = \frac{U_0}{k}\cos(kx)\cos(ky).$$

Adopting the usual change of variable $\mathbf{v} = \dot{\mathbf{r}}$, $\mathbf{v} = \mathbf{A}(\mathbf{r}) + \mathbf{w}$, we obtain

$$\tau\dot{\mathbf{v}} = \Gamma\mathbf{v} + \mathbf{A}(\mathbf{r}) + \sqrt{2D_0}\xi, \tag{13}$$

where the matrix Γ assumes the simple form:

$$\Gamma(\mathbf{r}) = \mathscr{J} - \tau\nabla\mathbf{A}(\mathbf{r}), \tag{14}$$

and $\mathscr{J}$ is the identity matrix. For those values of τ such that the matrix Γ is no longer positive-defined, the overdamped limit needed for UCNA becomes meaningless. We recall that a diagonalizable matrix is positive-defined when all its eigenvalues are positive. The eigenvalues of the matrix Γ (eqn (14)) read:

$$\lambda_1 = 1 - \tau k^2\sqrt{\phi^2 - \psi^2}$$

$$\lambda_2 = 1 + \tau k^2\sqrt{\phi^2 - \psi^2}.$$

Using the definition of $\psi(x,y)$ and $\phi(x,y)$, after some algebraic manipulations, we obtain

$$\lambda_1 = 1 - \tau k U_0\sqrt{\cos[k(x-y)]\cos[k(x+y)]}$$

$$\lambda_2 = 1 + \tau k U_0\sqrt{\cos[k(x-y)]\cos[k(x+y)]}$$

When $\tau \geq \tau^* = 1/(U_0k)$, the eigenvalue λ_1 has no possibility to remain positive all over the plane (x,y), then Γ cannot be positive definte, and the overdamped regime turns to be undefined. In the opposite regime, $\tau < \tau^*$, which we call small-τ limit, the overdamped regime could be assumed. Only, in the latter case, the dynamics can be recast onto:

$$\Gamma\mathbf{v} = \mathbf{A}(\mathbf{r}) + \sqrt{2D_0}\xi. \tag{15}$$

By inversion we obtain:

$$\dot{\mathbf{r}} = \mathbf{v} = \Gamma^{-1}\Big(\mathbf{A}(\mathbf{r}) + \sqrt{2D_0}\xi\Big), \tag{16}$$

which corresponds to the UCNA dynamics[80] adapted to the current case.

We remark that τ^* roughly corresponds to the value of τ at which D_{eff} starts to change consistently with respect to the Shraiman's prediction, as shown in Fig. 3.

B Variation of the flow-field parameters

In this appendix, we show the effect of the flow-field parameters, L and U_0, on the transport properties of self-propelled particles in a laminar flow, justifying the choice to set $L = U_0 = 1$ in our study.

Rescaling the variables of the dynamics with the parameters of the flow-field, *i.e.* introducing dimensionless variables:

$$\mathbf{r} = \tilde{\mathbf{r}}L, \quad t = \tilde{t}T_{\mathrm{U}} = \tilde{t}\frac{L}{U_0}, \tag{17}$$

$$\mathbf{w} = \tilde{\mathbf{w}}U_0, \quad \xi = \frac{\tilde{\xi}}{\sqrt{T_{\mathrm{U}}}} = \tilde{\xi}\frac{\sqrt{U_0}}{\sqrt{L}}, \tag{18}$$

the dynamics (1) can be recast onto:

$$\dot{\tilde{\mathbf{r}}} = \mathbf{a}(\tilde{\mathbf{r}}) + \tilde{\mathbf{w}} \tag{19}$$

where $\mathbf{a}(\tilde{\mathbf{r}}) = (\sin(2\pi\tilde{x})\cos(2\pi\tilde{y}), -\cos(2\pi\tilde{x})\sin(2\pi\tilde{y}))$. Eqn (19) no longer contains any parameter dependence which, instead, is contained in the active force dynamics:

$$\tilde{\tau}\dot{\tilde{\mathbf{w}}} = -\tilde{\mathbf{w}} + \sqrt{2\tilde{D}_0}\tilde{\xi}. \tag{20}$$

Now, the dot indicates the time derivative with respect to the rescaled time $\tilde{t}$ and, in analogy with eqn (2), we have introduced the dimensionless persistence time, $\tilde{\tau}$, and the dimensionless diffusion coefficient, $\tilde{D}_0$:

$$\tilde{\tau} = \frac{\tau}{T_{\mathrm{U}}} = \tau\frac{U_0}{L}, \tag{21}$$

$$\tilde{D}_0 = \frac{D_0}{LU_0}. \tag{22}$$

As a consequence, the variations of L and U_0 can be mapped onto a change of $\tilde{\tau}$ and $\tilde{D}_0$, since the dynamics is only controlled by the ratios (21) and (22). In particular, the growth of L induces a simultaneous decrease of $\tilde{D}_0$ and $\tilde{\tau}$, while the increase of U_0 produces the decrease of $\tilde{D}_0$ but the growth of $\tilde{\tau}$. This observation justifies our numerical study obtained with $U_0 = L = 1$.

For the sake of completeness, in Fig. 6, we report D_{eff} *vs.* L at fixed U_0 (main panel) and D_{eff} *vs.* U_0 at fixed L (inset), keeping fixed $\tau = D_0 = 1$. The data reported correspond to those of Fig. 3 and 4, with the same values of $\tilde{\tau}$ and $\tilde{D}_0$.

C Computation of t_s in the regime of large τ

The typical time t_s contained in eqn (8) and (9) can be obtained by integrating eqn (1) without the self-propulsion in a given direction along a separatrix, for instance:

$$t_s = \frac{1}{U_0}\int_0^{L/2}\frac{\mathrm{d}x}{\sin(2\pi x/L)}. \tag{23}$$

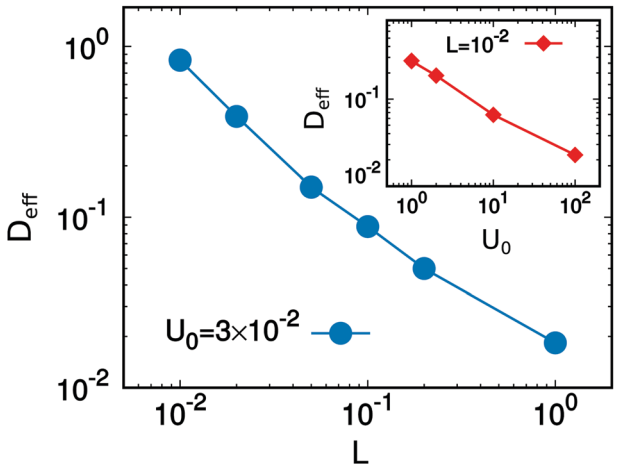

Fig. 6 In the main panel, we plot the effective diffusion coefficient, D_{eff}, *vs.* L for $U_0 = 3 \times 10^{-2}$, while in the inset, we show D_{eff} *vs.* U_0. In both cases, simulations are realized keeping fixed $\tau = 1$ and $D_0 = 1$.

This procedure is justified because the active force is negligible along the separatrices, except for the nodes, in the large persistence regime. The integral defining t_s is not converging, unless we introduce two cut-offs

$$t_s = \frac{1}{U_0}\int_{x_m}^{L/2-x_m} \frac{dx}{\sin(2\pi x/L)}. \quad (24)$$

The length scale x_m is chosen such as:

$$U_0 \sin(k x_m) = \sqrt{2b\frac{D_0}{\tau}}, \quad (25)$$

i.e. when the force along a separatrix is roughly equal to the typical value of the activity, estimated by its standard deviation, $\sqrt{D_0/\tau}$. The factor b is a parameter that does not depend on τ, D_0 and T_U, being just a numerical factor. Inverting eqn (25), we get

$$x_m = \frac{L}{2\pi}\arcsin\left(\sqrt{\frac{2bD_0}{\tau}}\frac{1}{U_0}\right) \approx \frac{L}{U_0\pi}\sqrt{\frac{bD_0}{2\tau}},$$

where we used the condition $\sqrt{D_0/\tau} \ll U_0 = 1$, holding in the large persistence regime. Solving the integral, we obtain the final expression for t_s,

$$t_s\frac{U_0\pi}{L} = \log\left(\frac{1}{\tan\left[\sqrt{\frac{bD_0}{2\tau}}\frac{1}{U_0}\right]}\right) \approx \frac{1}{2}\log\left(\frac{2U_0^2}{b}\frac{\tau}{D_0}\right),$$

which is positive since $U_0\sqrt{\tau/D_0} \gg 1$. Thus, t_s contains a logarithmic dependence on D_0/τ, as reported in eqn (9).

Acknowledgements

We thank A. Vulpiani and A. Crisanti for useful discussions. L. Caprini, F. Cecconi, A. Puglisi and A. Sarracino acknowledge support from the MIUR PRIN 2017 project 201798CZLJ. A. Sarracino acknowledges support from Program (VAnviteLli pEr la RicErca: VALERE) 2019 financed by the Univeristy of Campania "L. Vanvitelli". F. Cecconi and A. Puglisi acknowledge the financial support of Regione Lazio through the Grant "Progetti Gruppi di Ricerca" No. 85-2017-15257.

Notes and references

1 C. Bechinger, R. Di Leonardo, H. Löwen, C. Reichhardt, G. Volpe and G. Volpe, *Rev. Mod. Phys.*, 2016, **88**, 045006.
2 M. C. Marchetti, J. F. Joanny, S. Ramaswamy, T. B. Liverpool, J. Prost, M. Rao and R. A. Simha, *Rev. Mod. Phys.*, 2013, **85**, 1143–1189.
3 I. Buttinoni, J. Bialké, F. Kümmel, H. Löwen, C. Bechinger and T. Speck, *Phys. Rev. Lett.*, 2013, **110**, 238301.
4 J. Palacci, S. Sacanna, A. Steinberg, D. Pine and P. Chaikin, *Science*, 2013, **339**, 936–940.
5 F. Ginot, I. Theurkauff, F. Detcheverry, C. Ybert and C. Cottin-Bizonne, *Nat. Commun.*, 2018, **9**, 696.
6 Y. Fily and M. C. Marchetti, *Phys. Rev. Lett.*, 2012, **108**, 235702.
7 J. Bialké, T. Speck and H. Löwen, *J. Non-Cryst. Solids*, 2015, **407**, 367–375.
8 M. E. Cates and J. Tailleur, *Annu. Rev. Condens. Matter Phys.*, 2015, **6**, 219–244.
9 P. Digregorio, D. Levis, A. Suma, L. F. Cugliandolo, G. Gonnella and I. Pagonabarraga, *Phys. Rev. Lett.*, 2018, **121**, 098003.
10 A. P. Solon, J. Stenhammar, M. E. Cates, Y. Kafri and J. Tailleur, *New J. Phys.*, 2018, **20**, 075001.
11 P. Chiarantoni, F. Cagnetta, F. Corberi, G. Gonnella and A. Suma, *J. Phys. A: Math. Theor.*, 2020, accepted.
12 L. Caprini, U. M. B. Marconi and A. Puglisi, *Phys. Rev. Lett.*, 2020, **124**, 078001.
13 K.-D. N. T. Lam, M. Schindler and O. Dauchot, *New J. Phys.*, 2015, **17**, 113056.
14 F. Ginelli, F. Peruani, M. Bär and H. Chaté, *Phys. Rev. Lett.*, 2010, **104**, 184502.
15 Y. Sumino, K. H. Nagai, Y. Shitaka, D. Tanaka, K. Yoshikawa, H. Chaté and K. Oiwa, *Nature*, 2012, **483**, 448.
16 B. ten Hagen, S. van Teeffelen and H. Löwen, *J. Phys.: Condens. Matter*, 2011, **23**, 194119.
17 F. J. Sevilla and L. A. G. Nava, *Phys. Rev. E: Stat., Nonlinear, Soft Matter Phys.*, 2014, **90**, 022130.
18 U. Basu, S. N. Majumdar, A. Rosso and G. Schehr, *Phys. Rev. E*, 2018, **98**, 062121.
19 C. Scholz, S. Jahanshahi, A. Ldov and H. Löwen, *Nat. Commun.*, 2018, **9**, 1–9.
20 F. J. Sevilla and P. Castro-Villarreal, 2019, arXiv preprint arXiv:1912.03425.
21 L. Caprini and U. M. B. Marconi, *Soft Matter*, 2019, **15**, 2627–2637.
22 G. Miño, M. Baabour, R. Chertcoff, G. Gutkind, E. Clément, H. Auradou and I. Ippolito, *Adv. Microbiol.*, 2018, **8**, 451–464.

23 G. Li and J. X. Tang, *Phys. Rev. Lett.*, 2009, **103**, 078101.
24 H. Wensink and H. Löwen, *Phys. Rev. E*, 2008, **78**, 031409.
25 J. Elgeti and G. Gompper, *Europhys. Lett.*, 2013, **101**, 48003.
26 R. Wittmann and J. M. Brader, *EPL*, 2016, **114**, 68004.
27 S. Das, S. Ghosh and R. Chelakkot, *arXiv preprint arXiv:2001.04654*, 2020.
28 L. Caprini, F. Cecconi and U. Marini Bettolo Marconi, *J. Chem. Phys.*, 2019, **150**, 144903.
29 R. M. Ford and R. W. Harvey, *Adv. Water Resour.*, 2007, **30**, 1608–1617.
30 M. Engstler, T. Pfohl, S. Herminghaus, M. Boshart, G. Wiegertjes, N. Heddergott and P. Overath, *Cell*, 2007, **131**, 505–515.
31 D. Ribet and P. Cossart, *Microbes Infect.*, 2015, **17**, 173–183.
32 O. Chepizhko and F. Peruani, *Phys. Rev. Lett.*, 2013, **111**, 160604.
33 O. Chepizhko, E. G. Altmann and F. Peruani, *Phys. Rev. Lett.*, 2013, **110**, 238101.
34 T. Majmudar, E. E. Keaveny, J. Zhang and M. J. Shelley, *J. R. Soc., Interface*, 2012, **9**, 1809–1823.
35 A. T. Brown, I. D. Vladescu, A. Dawson, T. Vissers, J. Schwarz-Linek, J. S. Lintuvuori and W. C. Poon, *Soft Matter*, 2016, **12**, 131–140.
36 G. Volpe, I. Buttinoni, D. Vogt, H.-J. Kümmerer and C. Bechinger, *Soft Matter*, 2011, **7**, 8810–8815.
37 M. Khatami, K. Wolff, O. Pohl, M. R. Ejtehadi and H. Stark, *Sci. Rep.*, 2016, **6**, 37670.
38 C. Sándor, A. Libál, C. Reichhardt and C. Olson Reichhardt, *J. Chem. Phys.*, 2017, **146**, 204903.
39 A. Kaiser, H. Wensink and H. Löwen, *Phys. Rev. Lett.*, 2012, **108**, 268307.
40 J. Tailleur and M. Cates, *EPL*, 2009, **86**, 60002.
41 M. Wan, C. O. Reichhardt, Z. Nussinov and C. Reichhardt, *Phys. Rev. Lett.*, 2008, **101**, 018102.
42 G. Volpe, S. Gigan and G. Volpe, *Am. J. Phys.*, 2014, **82**, 659–664.
43 P. Galajda, J. Keymer, P. Chaikin and R. Austin, *J. Bacteriol.*, 2007, **189**, 8704–8707.
44 O. Bénichou, P. Illien, G. Oshanin, A. Sarracino and R. Voituriez, *Phys. Rev. Lett.*, 2015, **115**, 220601.
45 T. Jakuszeit, O. A. Croze and S. Bell, *Phys. Rev. E*, 2019, **99**, 012610.
46 S. Pattanayak, R. Das, M. Kumar and S. Mishra, *Eur. Phys. J. E: Soft Matter Biol. Phys.*, 2019, **42**, 62.
47 C. Reichhardt and C. O. Reichhardt, *Phys. Rev. E*, 2018, **97**, 052613.
48 A. Morin, N. Desreumaux, J.-B. Caussin and D. Bartolo, *Nat. Phys.*, 2017, **13**, 63–67.
49 M. Zeitz, K. Wolff and H. Stark, *Eur. Phys. J. E: Soft Matter Biol. Phys.*, 2017, **40**, 23.
50 J. L. Aragones, S. Yazdi and A. Alexander-Katz, *Phys. Rev. Fluids*, 2018, **3**, 083301.
51 E. Barkai, Y. Garini and R. Metzler, *Phys. Today*, 2012, **65**, 29.
52 M. R. Shaebani, Z. Sadjadi, I. M. Sokolov, H. Rieger and L. Santen, *Phys. Rev. E: Stat., Nonlinear, Soft Matter Phys.*, 2014, **90**, 030701.
53 E. Woillez, Y. Kafri and N. Gov, *Phys. Rev. Lett.*, 2019, **124**, 118002.
54 B. I. Shraiman, *Phys. Rev. A: At., Mol., Opt. Phys.*, 1987, **36**, 261.
55 G. I. Taylor, *Proc. R. Soc. London, Ser. A*, 1953, **219**, 186–203.
56 S. Thorpe, *Annu. Rev. Fluid Mech.*, 2004, **36**, 55–79.
57 R. Alonso-Matilla, B. Chakrabarti and D. Saintillan, *Phys. Rev. Fluids*, 2019, **4**, 043101.
58 W. M. Durham, E. Climent, M. Barry, F. D. Lillo, G. Boffetta, M. Cencini and R. Stocker, *Nat. Commun.*, 2013, **4**, 2148.
59 F. Santamaria, F. D. Lillo, M. Cencini and G. Boffetta, *Phys. Fluids*, 2014, **26**, 111901.
60 R. Rusconi, J. S. Guasto and R. Stocker, *Nat. Phys.*, 2014, **10**, 212–217.
61 G. Junot, N. Figueroa-Morales, T. Darnige, A. Lindner, R. Soto, H. Auradou and E. Clément, *EPL*, 2019, **126**, 44003.
62 P. Castiglione and A. Crisanti, *Phys. Rev. E: Stat., Nonlinear, Soft Matter Phys.*, 1999, **59**, 3926.
63 C. Torney and Z. Neufeld, *Phys. Rev. Lett.*, 2007, **99**, 078101.
64 A. Sarracino, F. Cecconi, A. Puglisi and A. Vulpiani, *Phys. Rev. Lett.*, 2016, **117**, 174501.
65 F. Cecconi, A. Puglisi, A. Sarracino and A. Vulpiani, *Eur. Phys. J. E: Soft Matter Biol. Phys.*, 2017, **40**, 81.
66 F. Cecconi, A. Puglisi, A. Sarracino and A. Vulpiani, *J. Phys.: Condens. Matter*, 2018, **30**, 264002.
67 J.-C. Wu, M. An and W.-G. Ma, *Soft Matter*, 2019, **15**, 7187–7194.
68 B.-q. Ai, W.-j. Zhu, Y.-f. He and W.-r. Zhong, *J. Chem. Phys.*, 2018, **149**, 164903.
69 W.-J. Zhu, Y.-L. He and B.-Q. Ai, *J. Stat. Mech.: Theory Exp.*, 2019, 103208.
70 Y. Li, L. Li, F. Marchesoni, D. Debnath and P. K. Ghosh, *Phys. Rev. Res.*, 2020, **2**, 013250.
71 S. Das, G. Gompper and R. Winkler, *New J. Phys.*, 2018, **20**, 015001.
72 E. Fodor, C. Nardini, M. E. Cates, J. Tailleur, P. Visco and F. van Wijland, *Phys. Rev. Lett.*, 2016, **117**, 038103.
73 L. Caprini, U. M. B. Marconi, A. Puglisi and A. Vulpiani, *J. Stat. Mech.: Theory Exp.*, 2019, 053203.
74 R. Wittmann, F. Smallenburg and J. M. Brader, *J. Chem. Phys.*, 2019, **150**, 174908.
75 L. Berthier, E. Flenner and G. Szamel, *J. Chem. Phys.*, 2019, **150**, 200901.
76 E. Woillez, Y. Kafri and V. Lecomte, *arXiv preprint arXiv:1912.04010*, 2019.
77 U. M. B. Marconi, N. Gnan, M. Paoluzzi, C. Maggi and R. Di Leonardo, *Sci. Rep.*, 2016, **6**, 23297.
78 C. Maggi, M. Paoluzzi, N. Pellicciotta, A. Lepore, L. Angelani and R. Di Leonardo, *Phys. Rev. Lett.*, 2014, **113**, 238303.
79 C. Maggi, M. Paoluzzi, L. Angelani and R. Di Leonardo, *Sci. Rep.*, 2017, **7**, 1–7.
80 C. Maggi, U. M. B. Marconi, N. Gnan and R. Di Leonardo, *Sci. Rep.*, 2015, **5**, 10742.
81 L. Caprini, U. M. B. Marconi and A. Puglisi, *Sci. Rep.*, 2019, **9**, 1386.
82 L. Caprini, U. M. B. Marconi, A. Puglisi and A. Vulpiani, *J. Chem. Phys.*, 2019, **150**, 024902.
83 R. L. Honeycutt, *Phys. Rev. A: At., Mol., Opt. Phys.*, 1992, **45**, 600.
84 L. Caprini, E. Hernández-Garcìa, C. López and U. M. B. Marconi, *Sci. Rep.*, 2019, **9**, 1–13.

